https://doi.org/10.24867/GRID-2026-p92

# A Case Study in Auxetic Structure Design for an Adaptive 3D-Printed Handbag

**ABSTRACT**

*Everyday products such as handbags have fixed geometries that cannot adapt to changing loads. Auxetic lattices, which expand laterally when stretched, offer one route to adaptive form, but they have mainly been explored in engineering and wearable-tech contexts rather than in everyday consumer products. This paper presents a case study applying auxetic design to a 3D-printed handbag. Using Rhino and Grasshopper with the Linketix plugin, we built a parametric tote whose four planar walls carry a rotating-unit auxetic pattern driven by a single deployment parameter. A quadrilateral (rotating-square) configuration was developed into a complete bag, with hinge necks between cells and handle attachment holes and rings located parametrically from the handle geometry so that the handles stay usable at every deployment state. A triangular configuration was generated at lattice level for comparison. A prototype of the bag body, without handles or rings, was printed in a flexible TPU and tested by hand to assess expansion and shape recovery. This case study offers an initial, concrete example of how load-responsive auxetic structures might be applied to adaptive consumer products, and as a starting point for a more general design workflow to be developed in future work.*

Athina Tziarou [1]
Panagiota Ligka [1]
Nikolla Vesho [2]
Panagiotis Kyratsis [1]

[1] Department of Product and Systems Design Engineering, University of Western Macedonia, Koila, Western Macedonia
[2] Polis University, Tirana, Albania

**KEY WORDS**
Auxetic structures, negative Poisson's ratio, 3D printing, TPU, parametric design, Grasshopper, adaptive products, handbag design

## 1. Introduction

Consumer products such as handbags are designed with static geometries that do not change in response to varying contents or loads. This fixed design can limit comfort, ergonomics, and functional adaptability in daily use. Auxetic metamaterials and structures with a negative Poisson's ratio, which expand laterally when stretched, can offer a pathway to create load-responsive, adaptive forms. While auxetics have been studied extensively in aerospace, biomedical, sports, and textile applications, their use in everyday fashion accessories remains underexplored (Bagewadi et al., 2026).

This paper presents a case study that applies auxetic lattice design to a 3D-printed handbag, exploring how parametric modelling and flexible materials can enable adaptive geometry in a consumer product. The contribution is a practical, documented parametric workflow, including the failure points encountered, and empirical observations on cell-type behaviour in TPU, aiming to inform future adaptive product development (Shirzad et al., 2025).

## 2. Background and literature review

### 2.1. Auxetic Structures and Negative Poisson's Ratio

Auxetic materials exhibit a negative Poisson's ratio, meaning they expand in transverse directions when subjected to tensile loading, and contract when compressed (Bagewadi et al., 2026; Johnston & Kazanci, 2021). This behavior contrasts with conventional materials, which thin out when stretched. The phe-

nomenon arises from specific micro-architectures, such as re-entrant, chiral, or rotating unit geometries that reconfigure under load (Bagewadi et al., 2026; Farshbaf et al., 2025; Papadopoulou, Laucks & Tibbit, 2017).

Key mechanical advantages of auxetics include enhanced energy absorption, indentation resistance, fracture toughness, and conformability to complex surfaces (Junio et al., 2023; Sobreira, Ayres & Pagnan, 2024). These properties make them attractive for protective apparel, biomedical devices, sports equipment, and increasingly, wearable and fashion applications (Kabir et al., 2022; Papadopoulou et al., 2017; Sobreira, Ayres & Pagnan, 2024).

### 2.2. 3D Printing of Auxetic Lattices in Flexible Polymers

Additive manufacturing enables precise realization of complex auxetic geometries that would be difficult or impossible to produce with traditional methods (Bagewadi et al., 2026; Farshbaf et al., 2025). Thermoplastic polyurethane (TPU) is a popular flexible filament for 3D printing auxetic lattices due to its elasticity, durability, and ability to undergo repeated deformation (Farshbaf et al., 2025). Recent studies have investigated the mechanical properties of 3D-printed TPU lattice structures, including the effects of build orientation and loading direction (Beloshenko et al., 2023).

However, the extent to which existing research addresses standardized mechanical testing of flexible lattice structures and their application in consumer fashion products remains unclear.

### 2.3. Parametric Design with Grasshopper for Lattice Structures

Grasshopper, a visual scripting environment for Rhino 3D, enables the parametric generation and modification of lattice geometries. Parametric modelling is particularly useful for exploring different unit-cell configurations and adjusting geometric parameters, while research on 3D-printed auxetic metamaterials has also examined computational approaches to mechanical analysis (Garg et al., 2025). The parametric model allows rapid iteration between quadrilateral, triangular, and hexagonal cell geometries, supporting the comparison of different lattice configurations.

### 2.4. Auxetics in Fashion and Consumer Products

Although auxetic textiles and wearable components have been explored for clothing, footwear, and protective equipment, applications in fashion accessories such as handbags remain an area for further development. Existing research highlights the potential of auxetic materials in design and architecture, as well as their broader applications across product categories (Papadopoulou, Laucks & Tibbit, 2017; Sobreira, Ayres & Pagnan, 2024).

Research into auxetic componentry has also considered its potential in human-centred product design, highlighting the relevance of these structures to products that interact directly with users (Urquhart et al., 2024).

This gap motivates the present case study, which bridges auxetic metamaterial design with everyday product form and function.

## 3. Methods

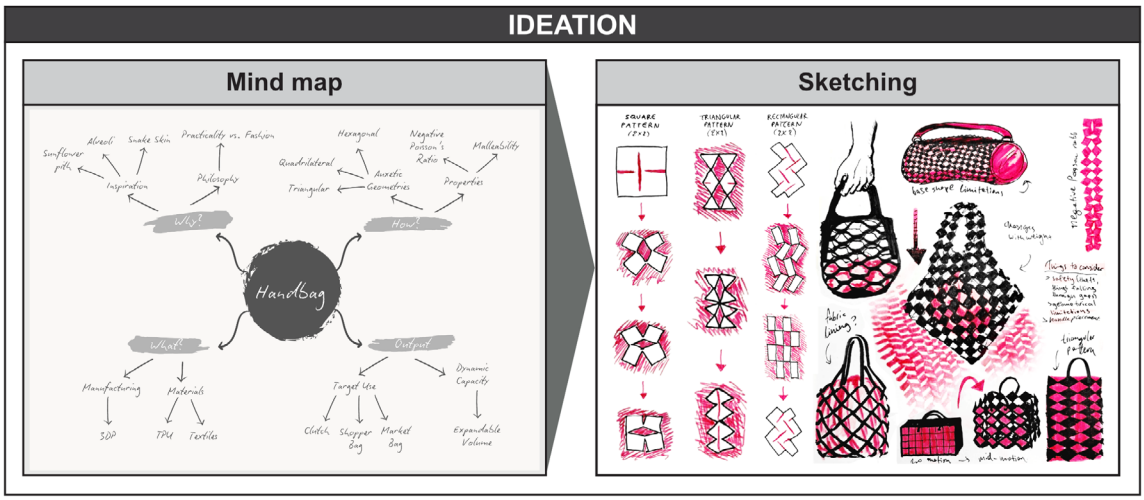
### 3.1. Workflow overview

The design was implemented parametrically in Rhinoceros 3D version 8 using Grasshopper™ and the Linketix auxetic-mechanism plugin. Custom Grasshopper Python components were written with the assistance of the Raven AI plugin, and the authors verified each stage by inspecting the resulting geometry and measured values. The workflow has six stages: (1) definition of a rectangular tote from four planar walls and a bottom, (2) generation of an auxetic pattern on each wall from a shared deployment parameter (Fig. 1), (3) conversion of the pattern into printable solids, (4) addition of hinge connections between cells, (5) parametric handle attachment, and (6) fabrication in flexible TPU and manual testing.

### 3.2. Bag form and pattern generation

The bag is a closed rectangular tote. Four vertical walls and a bottom cap are placed in the Grasshopper model with the walls on the XZ and YZ planes. At the current settings the unthickened envelope is *54.9 × 21.96 × 54.9 mm.* No surface mapping was used. Each wall gets its own pattern, generated flat on that wall's plane, which avoids the seam and strut-end problems that occurred when patterns were morphed onto a curved bag surface (Section 3.8).

Patterns were generated with the Linketix Rectangular 1 component. The component takes a plane, a cell length and width, the number of cells in each direction (Extent X and Extent Y) and a Motion value from 0 to 1 that deploys the pattern. Cell size equals the wall dimension divided by the cell count. The front and back walls use *5 × 5* cells (*100* cells each) and the side walls use *2 × 5* cells (*40* each), a total of *280* cells with a side length of *5.49 mm.* The back and right walls are mirrored copies of the front and left walls, and all walls share one Motion control. In the rest state (*Motion = 0*) the pattern is a plain square grid, and the re-entrant gaps open only as Motion increases.




» **Figure 1:** *Conceptual mind map and initial hand-drawn pattern iterations exploring auxetic handbag geometries and cell types*

## 3.3. Cell types

Linketix offers several auxetic generators. The quadrilateral configuration (Rectangular 1) was carried through to a complete bag. The triangular configuration (Linketix Triangular) was generated for comparison. It has no independent width input, so the cell length *L* was set from the panel width *W* and the number of cells in *X*, $n_X$:

$$L = \frac{W}{n_X\sqrt{3}} \quad (1)$$

and the number of rows in *Y*, $n_Y$, was set from the target panel height H and rounded to the nearest integer, because the generator only accepts whole numbers:

$$n_Y = round(\frac{H}{2L}) \quad (2)$$

For the front and back walls (*W = H = 54.9 mm*, $n_X$ = *5*), Eq. (1) gives *L = 6.339 mm* and Eq. (2) gives *4.33,* rounded to $n_Y$ *= 4.* This reproduces the *54.9 mm* panel width exactly but gives a height of *2L* $n_Y$ *= 50.714 mm, 7.6%* short, because of the integer rounding. The triangular lattice has *224* cells *(32 + 80 + 32 + 80).* A hexagonal configuration was not implemented.

## 3.4. Solid generation

Each cell outline was converted into a filled planar surface and extruded to a wall thickness of *1.4 mm,* giving *280* closed solids for the quad bag. The bottom is a rigid *1.4 mm* slab sized to the thickened wall footprint. It does not deploy, so the bottom row of cells is locally constrained. This is a deliberate trade-off: the base carries the load, and joining a deploying lattice to a fixed base through a second auxetic panel produces geometric collisions at the seam.

## 3.5. Hinge necks

At *Motion = 0* neighbouring cells share full edges, so the wall is effectively a solid sheet and the pattern has no hinge mechanism. At *Motion = 0.2* the cells are separated by edge gaps of about *1.6 mm* (digital measurement at edge midpoints) but touch only at zero-width corners, which cannot be printed. To keep the cells connected as a flexible structure, a *1.0 mm* diameter cylindrical neck spanning the wall thickness was added at every shared corner: *492* necks (front *180*, back *180*, left *66*, right *66*). A Python component checked that each neck overlaps both neighbouring cells, and each local cell-neck-cell union was confirmed to be a single closed manifold solid. The bag was therefore designed to be printed at *Motion = 0.2*, not at rest.

## 3.6. Handle attachment

Two handles were modelled as arcs piped at *1 mm* radius with a *12 mm* rise. To avoid fixing the handles to a lattice that deforms, four attachment cells (two front, two back) are selected parametrically, with no typed coordinates or fixed indices: the top-row cell surfaces of the front and back walls are merged into one list, the four handle endpoints are grafted into separate branches, a Surface Closest Point calculation measures distance from each endpoint to every surface, and a Sort List and List Item (*index 0*) returns the nearest cell for each endpoint. A *1.5 mm* radius hole is cut through each selected cell with a single Boolean difference (one cell at a time), and each result was checked to be a closed manifold solid. A slim ring passes through each hole and is joined to the handle end, so the handle moves freely relative to the lattice at any deployment state (Fig. 2). The handles and rings were designed and checked digitally only. They were not part of the printed prototype (Section 3.7), so their behaviour in use is untested.

## 3.7. Assembly, boolean limits and export

The complete digital assembly contains about 775 separate closed solids (280 cells, 492 hinge necks, the bottom, and the two handles; the rings add further solids). A single Solid Union of the full set returned an empty result in Grasshopper, even though all inputs were individually valid, so the parts were baked as separate objects and exported as one STL for the slicer to merge.

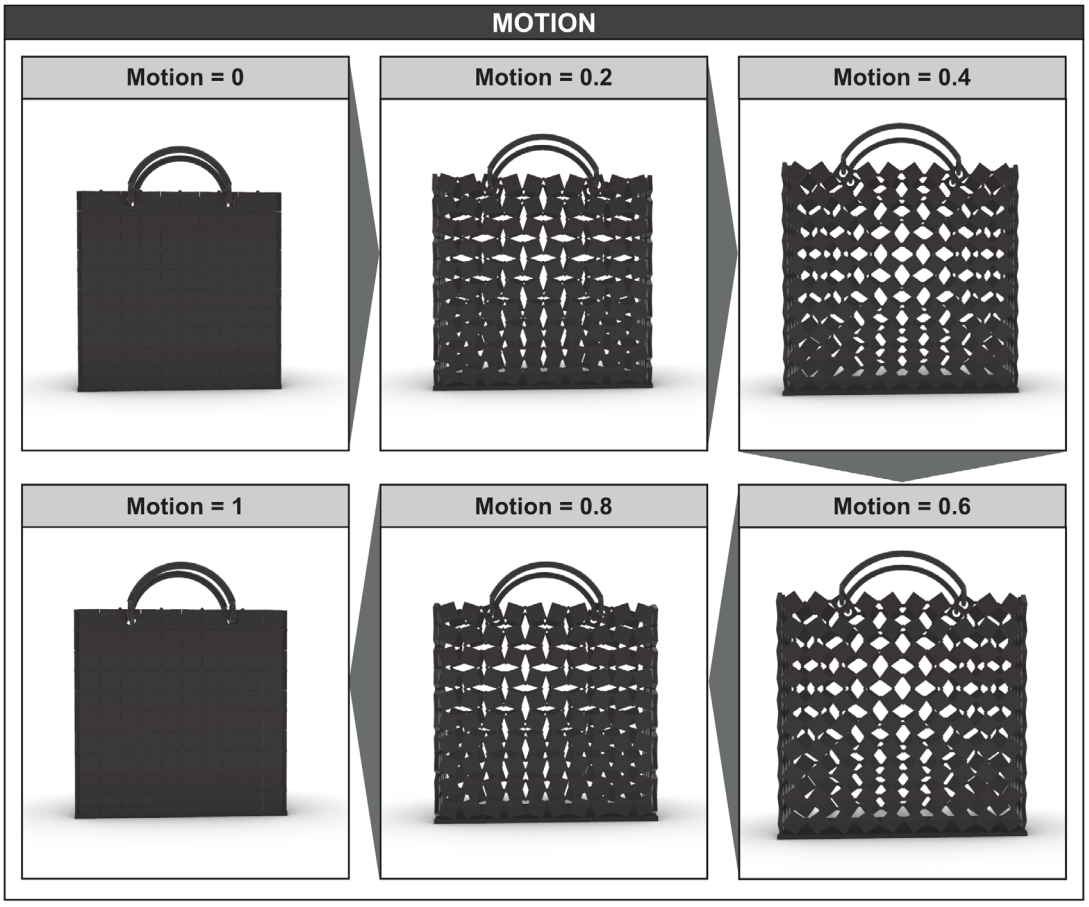
The printed prototype was the bag body only: the cells, hinge necks and bottom, about 773 solids, with the four attachment holes being part of the test print. The handles and rings were left out. The bag body was printed on a direct-drive FDM 3D printer using flexible TPU filament (Shore hardness 95A) with a *0.4 mm* nozzle. Printing parameters were set to a layer height of *0.2 mm*, a print speed of *30 mm/s*, and a nozzle temperature of *210°C.*

## 3.8. Design iterations and limitations

Several approaches were tried before the final design:

- Surface mapping: Mapping the lattice onto a tapered bag surface produced distorted and twisted loft geometry, so the bag was redesigned as a box with flat walls.
- Cell construction: An early cell definition built from per-panel morphs produced scale errors; a single plane-based generator per wall with cell size computed from the wall dimension replaced it.
- Rest state: Filled-cell walls fuse into a solid sheet at Motion = 0, which led to printing near *Motion = 0.2* and to the hinge necks.
- Handles: Handle geometry attached to fixed coordinates or a rigid band either broke the deformation or failed when Motion changed. Free rings through parametrically located holes replaced both.
- Triangular cells: The hinge-neck logic assumes every shared corner is shared by exactly two cells. Triangular tiling has four-cell junctions, so the hinge, assembly and ring stages were not carried over to the triangular bag.

Remaining limitations: (a) only the quad configuration is a complete printable bag; (b) the hexagonal configuration was not built; (c) Motion is a kinematic parameter, not a force, so the digital results are not loaded-response predictions; (d) the bottom cap does not deploy; (e) no instrumented testing; (f) no Boolean-clean single-solid export; (g) the handles and rings were not printed, so the handle-attachment concept is verified digitally




» **Figure 2:** *Parametric simulation of the quadrilateral handbag model showing continuous lateral expansion across a Motion value range from 0 to 1*

**Table 1**
Digital deployment of the front/back wall lattice for the two cell types

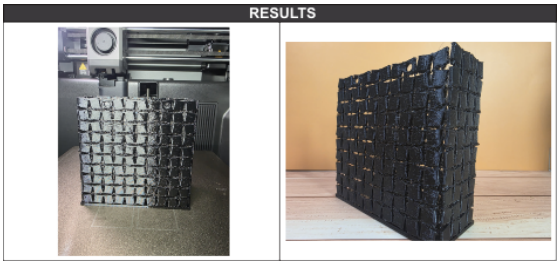
| Cell type | Width at Motion 0 | Width at Motion 0.3 | Width change | Height at Motion 0 | Height at Motion 0.3 | Height change |
|---|---|---|---|---|---|---|
| **Quadrilateral (Rectangular 1)** | 54.900 | 63.135 | +15.0% | 54.900 | 52.155 | -5.0% |
| **Triangular** | 54.900 | 59.183 | +7.8% | 50.714 | 50.090 | –1.2% |

only; (h) the single printed prototype experienced thermal sagging and stringing that caused adjacent cells to fuse, preventing physical testing, so the physical behaviour of the lattice is not established by this study.

# 4. Results

## 4.1. Digital deformation

The bounding-box width and height of the generated front/back wall lattice were measured in Grasshopper at *Motion = 0* and *Motion = 0.3* (Table 1). The side walls change by the same percentages in the triangular lattice (*+7.8%* width, *–1.23%* height). Similarly, the quadrilateral side walls exhibit a *+15.0%* increase in width and a *-5.0%* decrease in height at

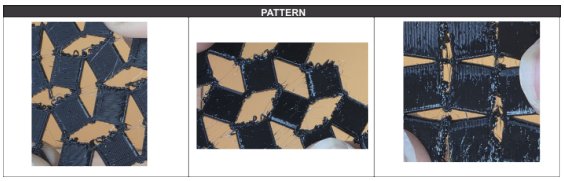



» **Figure 3:** *3D-printed TPU handbag prototype body (quadrilateral configuration) directly on the build bed (left) and standing (right)*

*Motion 0.3.* These are geometric measurements of the model, not physical expansion under load (Fig. 2).

## 4.2. Physical behaviour

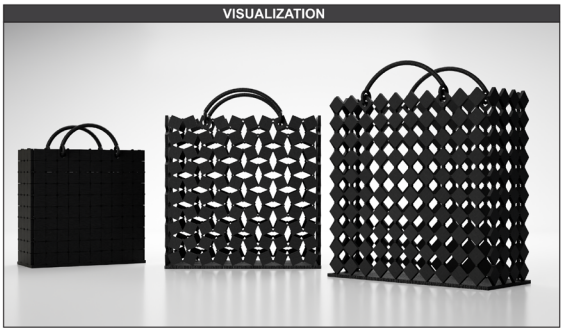
The bag body was printed once in flexible TPU, and at *Motion = 0.2*, as stated previously. Due to the extreme thinness of the *1.0 mm* hinge necks and the flexibility of the material, thermal sagging and stringing occurred during the print, causing adjacent cells to fuse partially together and preventing smooth articulation (Fig. 3, Fig. 4). Because of these localized fusion defects, the physical prototype could not be mechanically tested for live expansion or recovery. Because the print was not entirely successful, this study does not provide physical measurements of expansion or shape recovery, and the digital deployment in Table 1 is the only quantitative evidence of auxetic behaviour




» **Figure 4:** *Macro close-up views of the printed TPU quadrilateral lattice pattern showing cell separation, hinge necks, and stringing/fusion artifacts*

## 4.3. Handle attachment

The parametric attachment method found the correct cell for each handle endpoint, and all four 1.5 mm holes passed the closed-manifold check (about 9.9 mm³ of material removed per hole). Because the handles connect through free rings instead of being fixed to a cell, they are not tied to a specific deployment state. This is a digital result only: the handles and rings were not printed, so how they work in use remains untested (Fig. 5).




» **Figure 5:** *Final digital visualization of the complete handbag assembly featuring parametric handle integration and free-moving attachment rings across multiple deployment states*

# 5. Discussion

## 5.1. What the digital results show

The Motion parameter produces visible lateral opening in the triangular lattice (+7.8% width at Motion 0.3, with a small height loss), confirming auxetic-style deployment in the digital model. While the triangular lattice achieved a measurable +7.8% width expansion at Motion 0.3, the quadrilateral (rotating-square) configuration provides a simpler geometric pathway for future physical iterations, avoiding the complex four-way junction constraints encountered in triangular tiling (Bagewadi et al., 2026; Garg et al., 2025).

## 5.2. Design implications

The main practical findings are about the design process. Flat-walled forms were far easier to pattern parametrically than a tapered bag, and a lattice of filled cells needs explicit connection geometry (hinge necks) to be a connected structure rather than a solid sheet or a set of loose cells. Whether the 1.0 mm necks are strong and flexible enough in TPU was not established, because the printed prototype experienced thermal sagging and stringing that caused adjacent cells to fuse, preventing meaningful mechanical testing. Handles are best decoupled from a deforming lattice through free rings and holes, and attachment features should be located parametrically so they update as the pattern changes. The triangular lattice shows that hinge strategies developed for rotating-square cells do not carry over to cells with four-way junctions (Papadopoulou, Laucks & Tibbit, 2017; Sobreira, Ayres & Pagnan, 2024).

## 5.3. Limitations and Future Work

Limitations are listed in Section 3.8. Future work includes: reprinting the bag body with revised settings or neck dimensions, and printing the handles and rings; completing the hexagonal and triangular bags with a hinge approach that handles four-cell junctions; deploying the bottom cap; graded stiffness near the handles (for example attractor-driven cell size or thickness); instrumented force-displacement testing and optical strain analysis; FEM simulation of the cell mechanism; and extension to other products.

Future work should:

- Incorporate instrumented mechanical testing, including force-displacement sensors and optical strain analysis, to obtain more precise measurements of deformation and recovery.
- Explore hybrid materials, such as TPU combined with rigid inserts, to improve structural performance.
- Develop computational simulations, including finite element modeling (FEM), to predict auxetic behavior before printing (Garg et al., 2025).
- Extend the workflow to other product categories, including backpacks, footwear, and protective equipment, building on the wider design applications of auxetic materials (Sobreira, Ayres & Pagnan, 2024; Urquhart et al., 2024).

These directions could help establish a more systematic approach to designing, testing, and optimizing auxetic structures for everyday consumer products.

# 6. Conclusion

This paper presented a case study applying auxetic lattice design to a 3D-printed handbag. A parametric tote with deploying walls was built in Grasshopper with the Linketix plugin, developed into a complete bag with hinge necks, a rigid base and parametrically located handle attachments, and compared at lattice level with a triangular configuration. The first print of the bag body was unsuccessful due to thermal sagging and stringing that caused adjacent cells to fuse, so physical expansion and recovery remain to be tested in future work, as does the printed performance of the handle attachments. The documented workflow, including the failure points encountered, provides a starting point for adaptive consumer products with auxetic structures.

# 7. References

Bagewadi, S.S., Hiremath, V.S., Biradar, A.V. and Dhilipkumar, T. (2026) 'State-of-the-art in 3D printing of auxetic structures: Recent progress and perspectives', *Journal of Materials Science: Materials in Engineering*, 21(1), article 89. DOI: 10.1186/s40712-026-00465-2

Beloshenko, V., Beygelzimer, Y., Chishko, V., Savchenko, B., Sova, N., Verbylo, D. and Vozniak, I. (2023) 'Mechanical properties of thermoplastic polyurethane-based three-dimensional-printed lattice structures: Role of build orientation, loading direction, and filler', *3D Printing and Additive Manufacturing*, 10(2), pp. 245–255. DOI: 10.1089/3dp.2021.0031

Farshbaf, S., Dialami, N., Cervera, M., Bakhshan, H. and Chakherlou, T.N. (2025) 'Enhancing the mechanical performance of additively manufactured auxetic structures through design modifications: Experimental and numerical analysis', *Progress in Additive Manufacturing*, 10, pp. 4143–4164. DOI: 10.1007/s40964-025-01062-z

Garg, A., Sharma, A., Zheng, W. and Li, L. (2025) 'A review on artificial intelligence-enabled mechanical analysis of 3D printed and FEM-modelled auxetic metamaterials', *Virtual and Physical Prototyping*, 20(1), e2445712. DOI: 10.1080/17452759.2024.2445712

Johnston, R. and Kazanci, Z. (2021) 'Analysis of additively manufactured (3D printed) dual-material auxetic structures under compression', *Additive Manufacturing*, 38, article 101783. DOI: 10.1016/j.addma.2020.101783

Junio, R.F.P., da Silveira, P.H.P.M., Neuba, L.d.M., Monteiro, S.N. and Nascimento, L.F.C. (2023) 'Development and Applications of 3D Printing-Processed Auxetic Structures for High-Velocity Impact Protection: A Review', *Eng*, 4(1), pp. 903–940. DOI: 10.3390/eng4010054

Kabir, S., Li, Y., Salahuddin, M. and Lee, Y.-A. (2022) 'Drapability of 3D Printed Auxetic Structure Textiles for Wearable Products'. In: *International Textile and Apparel Association Annual Conference Proceedings*, 79(1), 26–29 October 2022, Denver, Colorado, USA. Ames, IA: Iowa State University Digital Press. DOI: 10.31274/itaa.15933

Papadopoulou, A., Laucks, J. and Tibbits, S. (2017) 'Auxetic materials in design and architecture', *Nature Reviews Materials*, 2(12), article 17078. DOI: 10.1038/natrevmats.2017.78

Shirzad, M., Chashmi, M.J., Khakzadkelarijani, S., Kang, J., Bodaghi, M. and Nam, S.Y. (2025) 'Machine-learning-assisted design and optimization of auxetic structures: A bioinspired approach to mimic natural tissues', *Advanced Engineering Materials*, 27(20), article 2500377. DOI: 10.1002/adem.202500377

Sobreira, M.A.S., Ayres, E. and Pagnan, C.S. (2024) 'Auxetic materials in design – applications and possibilities', *Research, Society and Development*, 13(10), e61131046901. DOI: 10.33448/rsd-v13i10.46901

Urquhart, L., Tamburrino, F., Neri, P., Wodehouse, A., Fingland, C. and Razionale, A.V. (2024) 'An examination of auxetic componentry for applications in human-centred biomedical product design settings', *International Journal on Interactive Design and Manufacturing*, 18(8), pp. 5457–5467. DOI: 10.1007/s12008-023-01682-1




© 2026 Authors. Published by the University of Novi Sad, Faculty of Technical Sciences, Department of Graphic Engineering and Design. This article is an open access article distributed under the terms and conditions of the Creative Commons Attribution license 4.0 Serbia (http://creativecommons.org/licenses/by/4.0/rs/).